NACA TN 3586

NATIONAL ADVISORY COMMITTEE FOR AERONAUTICS

TECHNICAL NOTE 3586

IMPINGEMENT OF WATER DROPLETS ON NACA 65A004 AIRFOIL AT 0° ANGLE OF ATTACK

By Rinaldo J. Brun and Dorothea E. Vogt

Lewis Flight Propulsion Laboratory
Cleveland, Ohio

Washington

November 1955

NATIONAL ADVISORY COMMITTEE FOR AERONAUTICS

TECHNICAL NOTE 3586

IMPINGEMENT OF WATER DROPLETS ON NACA 65A004 AIRFOIL AT 0° ANGLE OF ATTACK

By Rinaldo J. Brun and Dorothea E. Vogt

SUMMARY

The trajectories of water droplets in the air flowing past an NACA 65A004 airfoil at an angle of attack of 0° were determined. The amount of water in droplet form impinging on the airfoil, the area of droplet impingement, and the rate of droplet impingement per unit area on the airfoil surface were calculated from the trajectories and presented to cover a large range of flight and atmospheric conditions. These impingement characteristics are compared briefly with those previously reported for the same airfoil at angles of attack of 4° and 8°.

INTRODUCTION

The data presented herein are a continuation of the study reported in references 1 and 2 on the impingement of cloud droplets on a low-drag, thin airfoil. The airfoil studied in both the references cited and in this report is a 4-percent-thick symmetrical NACA 65A004 airfoil. In references 1 and 2 the impingement characteristics of the airfoil were reported with the airfoil set at angles of attack of 4° and 8°, respectively; whereas, the data herein apply for an angle of attack of 0°. The range of angle of attack studied in the three reports permits the evaluation of the impingement characteristics for most flight plans of interceptor, fighter, and other high-speed aircraft.

The trajectories of atmospheric water droplets about an NACA 65A004 airfoil at 0° angle of attack at subsonic velocities were calculated with the aid of a differential analyzer at the NACA Lewis laboratory. From the computed trajectories, the rate, distribution, and surface extent of impinging water were obtained and summarized in this report. The results are applicable under the following conditions: chord lengths from 2 to 20 feet; altitudes from 1000 to 35,000 feet; airplane speeds from 150 miles per hour to the flight critical Mach number; and droplet diameters from 5 to 100 microns.

SYMBOLS

The following symbols are used in this report:

d	droplet diameter, microns (micron = 3.28×10^{-6} ft)
K	inertia parameter, $1.704\times10^{-12}\frac{d^2U}{\mu L}$, dimensionless (density of water, 1.94 slugs/cu ft, included in constant)
L	airfoil chord length, ft
Re_0	free-stream Reynolds number with respect to droplet, $4.813\times10^{-6}\frac{d\rho_a U}{\mu}$, dimensionless
S	distance on surface of airfoil measured from leading-edge chord point, ratio to chord length
U	flight speed, mph
u	local air velocity, ratio to free-stream velocity
W	rate of water impingement per unit span of airfoil, lb/(hr)(ft span)
W_m	rate of total water impingement per unit span of airfoil, lb/(hr)(ft span)
W_β	local rate of water impingement, lb/(hr)(sq ft)
w	liquid-water content in cloud, g/cu m
x,y	rectangular coordinates, ratio to chord length
β	local impingement efficiency, $\frac{dy_0}{dS}$, dimensionless
μ	viscosity of air, slugs/(ft)(sec)
ρ_a	density of air, slugs/cu ft

Subscripts:

l	lower airfoil surface

s airfoil surface

u upper airfoil surface

0 free stream

RESULTS AND DISCUSSION

In order to obtain the extent of impingement and the rate of droplet impingement per unit area on the airfoil, the cloud-droplet trajectories with respect to the airfoil were determined. The method for calculating the droplet trajectories is described in reference 3. A solution of the differential equations that describe the droplet motion was obtained with the use of the mechanical analog (described in ref. 4) based on the principle of a differential analyzer. The air-flow field around the airfoil was obtained as discussed in references 2 and 3. The values of the surface velocities for the 65A004 airfoil, which are required in the flow-field determination, were calculated by the Douglas Aircraft Corporation for the Lewis laboratory (see fig. 1). Although the droplet trajectories were calculated for an incompressible flow field, the results of the calculations can be applied up to the flight critical Mach number (ref. 5).

The geometric chord line of the airfoil is oriented at an angle of 0° with the x-axis of the rectangular coordinate system, and the leading edge is placed at the origin of the coordinates, as shown in figure 2. The airfoil orientation presented in references 1 and 2 is retained herein, except for the magnitude of the angle of attack. At an infinite distance ahead of the airfoil, the uniform air flow carrying the cloud droplets is assumed to be approaching the airfoil from the negative x-direction and parallel to the x-axis. All distances are given as dimensionless ratios, because they are ratios of the respective actual distance to the airfoil chord length L.

Rate of Total Water Interception

The rate of total water interception, in pounds per hour per foot of wing span, is determined by the tangent droplet trajectories (fig. 2), by the speed of the aircraft, and by the liquid-water content in the cloud. The flight speed and size of the airfoil, as well as the droplet size in the cloud, are the principal variables that affect the spacing between the two tangent trajectories. The amount of water that strikes the airfoil is proportional to the spacing $y_{0,u} - y_{0,l}$, and the rate of

total water interception per unit span of the airfoil on that portion of the airfoil surface bounded by the upper and lower tangent trajectories can be calculated from the relation

$$W_m = 0.33UwL(y_{0,u} - y_{0,l}) \quad (1)$$

The values of $y_{0,u} - y_{0,l}$ are given in figure 3 in terms of the reciprocal of the inertia parameter $1/K$ and the free-stream Reynolds number Re_0. The inertia parameter K is a measure of the droplet size, the flight speed and size of the airfoil, and the viscosity of the air through the relation

$$K = 1.704 \times 10^{-12} \frac{d^2U}{\mu L} \quad (2)$$

The density of water and the acceleration of gravity, which are expressed as part of the conversion factor, are 62.4 pounds per cubic foot and 32.17 feet per second per second, respectively. The free-stream Reynolds number is defined with respect to the droplet as

$$Re_0 = 4.813 \times 10^{-6} \frac{d\rho_a U}{\mu} \quad (3)$$

A graphical procedure for determining values of the dimensionless parameters K and Re_0 in terms of airplane speed, chord length, altitude, and droplet size is presented in appendix B of reference 3.

The variation of total rate of water interception with airfoil speed is summarized for an altitude of 20,000 feet in figure 4, in which the ordinate W_m/w is the total rate of water impingement per foot span of airfoil per unit liquid-water content (g/cu m) in the cloud. Several chord lengths ranging in value from 2 to 20 feet are considered. The values in figure 4 are for flight through clouds composed of uniform droplets 15, 20, 30, and 40 microns in diameter. The values of W_m/w given in figure 4 are based on the most probable icing temperature as a function of altitude presented in figure 15 of reference 3. (The most probable icing temperature was obtained from approximately 300 icing observations in flights.) As shown in reference 3, a change in altitude of 10,000 feet will change the rate of water impingement by approximately 7 percent. The droplet size and the liquid-water content of clouds are seldom known with sufficient accuracy (ref. 4) to permit the rate of water impingement to be calculated within 10 percent; therefore, within practical limits of application, the results of figure 4 can be used over a wide range of altitudes (approx. ±10,000 ft, see ref. 3).

The effect of wing taper can also be obtained from figure 4, provided that for each section of span considered the taper is small enough that two-dimensional flow over the section is approximated, as is mentioned in reference 3.

Extent of Impingement

The limit of impingement is determined by the point of tangency on the airfoil surface of the two tangent trajectories. The rearward limits of impingement on the upper and lower surface are shown in figure 5. Because the airfoil is symmetrical at an angle of attack of 0°, the limit of impingement on the lower surface is equal to that on the upper surface. The distances S_u and S_l are measured on the airfoil surface from the point of intersection of the geometric chord line with the leading edge (fig. 2) in terms of the chord length. The limits of impingement are given in figure 5 in terms of the reciprocal of the inertia parameter and free-stream Reynolds number.

Uncertainties in the location of the tangency point, and therefore in the magnitude of the limit of impingement, were discussed in references 1 and 2 for the airfoil placed at angles of attack of 4° and 8°, respectively. The uncertainties at 0° angle of attack are not as large as reported in the two references cited, because, generally, the tangent trajectories do not approach the airfoil surface as gradually at 0° as the lower surface is approached at either 4° or 8°. Also, 0° angle of attack permitted the use of a much larger scale factor in the y-ordinate of the calculating machine; thus, the point of tangency became more certain. The uncertainty in the location of the point of tangency is estimated to be less than ± 3 percent for the airfoil reported herein,

The surface limits are summarized in figure 6 for the same speeds, chord lengths, droplet sizes, and altitude given in figure 4.

Impingement Distribution on Surface

Trajectory starting ordinate as function of point of impact. - The manner in which water is distributed on the surface of an airfoil can be obtained if the starting point of a droplet trajectory is known with respect to the point of impingement on the surface. The starting ordinate y_0 at infinity of any impinging trajectory, including trajectories bounded by the upper and lower tangent trajectories (fig. 2), can be found in figure 7 with respect to the point of impingement on the surface. The values for the starting and ending positions of the trajectories are shown in figure 7 for four values of free-stream Reynolds number. For each value of Re_0, curves for several values of $1/K$ are given.

At an angle of attack of 0° the airfoil and the impingement are symmetrical with respect to the chord line (also x-axis). For this reason, the data are presented in figure 7 for the upper surface only, whereas in references 1 and 2 the corresponding data at 4° and 8°, respectively, are presented for both the upper and lower surfaces. The values of y_0 obtained from the end points of each curve in figure 7 are the same as one-half the values given in figure 3. The tangent-trajectory values, which were used for figures 3 and 5, fall on the dashed termini curves of figure 7.

The amount of water impinging between any two given points on the airfoil surface may be found by applying the results of figure 7 in the following relation:

$$W = 0.33UwL(y_{0,1} - y_{0,2}) \tag{4}$$

Local rate of droplet impingement. - The local rate of droplet impingement per unit area of airfoil surface can be determined from the expression

$$W_\beta = 0.33Uw \frac{dy_0}{dS} = 0.33Uw\beta \tag{5}$$

which is related to equation (4). The values of the local impingement efficiency β as a function of the airfoil distance S are given in figure 8. These values were obtained from the slopes of the curves in figure 7.

As is discussed in reference 1, the values of β (fig. 8) are very sensitive to the shape of the y_0 against S curves (fig. 7). Because of the geometry of the sharp-nosed NACA 65A004 airfoil and the manner in which the trajectories approach the airfoil surface, small errors in the calculated trajectories result in considerable error in the slopes of the curves of figure 7. The possible error in the values of β, due to computational procedure, for surface positions other than near the stagnation point, is estimated in reference 1 to be somewhat less than ± 10 percent for the values reported therein. Because of improved techniques in the computational procedure, the values of β given in figure 8 herein are in error by somewhat less than ± 2 percent for surface positions other than within 1 percent of the surface distance where the peak values of β occur. Since the total water impinging is directly related to

$$y_{0,u} - y_{0,l} = \int_{-S_l}^{S_u} \beta \, dS \tag{6}$$

a check on the computational accuracy of the values of β in figure 8 was also obtained by comparing the area under each β curve with the values of $y_{0,u} - y_{0,l}$ given in figure 3. The area values checked within ±1 percent of the corresponding values for total water interception.

The maximum values of β at the stagnation point (S = 0) are very uncertain. At 0° angle of attack the maximum values of β can be expected to be high (approx. equal to 1) for a thin sharp-nosed airfoil such as the 65A004 studied. The area check used in figure 8 also indicates high values for β at S = 0.

Variation of Impingement with Angle of Attack

The effect of varying the angle of attack from 0° to 8° on impingement can be found by comparing the results of references 1 and 2 with the present study. Because a complete comparison that covers a wide range of flight and atmospheric conditions is beyond the scope of this report, the following limited comparison is made for a set of conditions that occur rather frequently. However, the choice of only a few sets of conditions for comparison is dangerous, because the relative importance of the different factors involved may change with other conditions not discussed.

The comparisons in this section at different angles of attack for the NACA 65A004 airfoil are all made for conditions established at 300 miles per hour, a chord length of 9.4 feet, and an altitude of 10,000 feet. The comparisons are made for three droplet diameters, 80, 25, and 8 microns, which result in values of $1/K$ of 1, 10, and 100, respectively.

Rate of total water impingement. - The variation of the difference between the upper and lower tangent trajectories, $y_{0,u} - y_{0,l}$, with change in angle of attack is shown in figure 9. The rate of total water impingement, which is proportional to $y_{0,u} - y_{0,l}$, increases rapidly with increase in angle of attack, especially for the large droplet. With the small droplets (8 microns), the area of impingement remains on the rounded portion of the leading edge while the airfoil angle of attack is changed from 0° to 4°. The influence of changes in the air-flow field on the trajectories that impinge is not appreciable with changes in angle between 0° and 4°, because the impinging trajectories are confined to a region near the stagnation line for those angles. Along the stagnation line the vertical components of air velocity are not large between 0° and 4°. With the large droplets (80 microns), because of the larger droplet inertia, the influence of the air-flow field on the trajectories

in changing the airfoil from 0° to 4° is even less than with the small droplets; but the airfoil shape and the amount of area presented to the impinging trajectories are considerably different, because the impingement occurs much farther back on the airfoil.

Between 4° and 8° the influence of change in flow field on the trajectories of small droplets is probably of the same order of importance as the change of physical geometry. Even for small droplets the impingement no longer occurs principally around the leading edge when the airfoil is raised to angles greater than 4°. The combined influences of change in air-flow field and physical geometry on the trajectories that impinge result in a greater increasing slope of the curve (in fig. 9) for small droplets when angle of attack is increasing between 4° and 8°. The slope of the curve for large droplets (80 microns) also increases with increasing angles of attack between 4° and 8°; however, because of the higher inertia of the droplets and because of the large initial slope of the curve, the increase in slope is not as large as for the small droplets.

Extent of impingement. - Because of the shape of the 65A004 airfoil (principally, because the airfoil is thin and the maximum thickness occurs near the midpoint), the impingement on the upper surface is of consequence only at very small angles of attack. As was discussed in reference 2, the extent of impingement on the upper surface is very small for both 4° and 8°. At 4° angle of attack, S_u is always less than 0.02 for values of $1/K > 1$; and, at 8° angle of attack, S_u is always less than 0.01 for values of $1/K > 1$. At 0° angle of attack, $S_u = S_l$ and, as is seen in figure 5, ranges from 0.26 to 0.004 for $1 < 1/K < 100$.

The lower-surface limit is summarized in figure 10 for the same flight and atmospheric conditions given in figure 9. The change in shape of the curves as the droplet size is increased is explained in the following manner: As the angle of attack of the thin airfoil is increased, the airfoil presents itself to the droplets in the cloud ahead more as a flat plate without thickness than as a streamlined 4-percent-thick airfoil. Thus, the effect of a convex lower surface on impingement is minimized as the angle of attack is increased. For a flat plate of zero thickness, the impingement extends to the trailing edge ($S_l = 1$) for all values of K and Re_0 at all angles other than zero. When the convexity of the lower surface of the airfoil is no longer an important geometrical factor in determining the limit, the impingement extends to the trailing edge ($S_l \approx 1$) for all sizes of droplets. For small angles of attack the limit is very sensitive to the airfoil shape on the surface locality where the limit occurs. If, for example, the limit for the 8-micron droplet occurs at $S_l = 0.04$ at 4° angle of attack, a very small change in shape (or rate of change of curvature) of the airfoil surface in that neighborhood will change the limit considerably. At the same angle of attack the

limit for the 80-micron droplets is 0.53. The difference in the shape of the airfoil in the neighborhood of $S_l = 0.53$ compared with the shape in the neighborhood of $S_l = 0.04$, along with the difference in angle of approach of the trajectories to the surface at the two positions, accounts for the difference in the shape of the two curves.

The preceding discussion on the difference in the shape of the three curves in figure 10 may be summarized as follows: The limit of impingement is very sensitive to the physical geometry that the airfoil presents to the impinging trajectories, as well as to the pattern of the air streamlines around the airfoil. For this reason, limits of impingement determined for one airfoil shape should be used for another airfoil shape only with extreme caution.

Local rate of droplet impingement. - The maximum local rate of impingement occurs very nearly at $S = 0$ for all angles of attack up to 8°. The manner of distribution varies considerably with angle of attack. At 0° the water is evenly divided on the upper and lower surface. At 4° the amount of water impinging on the upper surface is a very small portion of the total, and at 8° the amount is nil. In the design of ice-protective systems, the upper surface protection should be designed for low angles of attack and the lower surface protection for the higher angles of attack encountered. At all angles of attack, the higher rates of local impingement are near the leading edge.

CONCLUDING REMARKS

The calculated data presented herein apply directly to flights in clouds composed of droplets that are all uniform in size and to nonswept wings of high aspect ratio. A detailed procedure for weighting the impingement of droplets for flights in nonuniform clouds is presented in reference 4. A method for extending the impingement calculations for nonswept wings to swept wings is presented in reference 6. As is discussed in reference 5, the impingement results should be applicable for most engineering uses throughout the subsonic region, because the subsonic compressibility of air does not affect the droplet trajectories appreciably.

Lewis Flight Propulsion Laboratory
National Advisory Committee for Aeronautics
Cleveland, Ohio, September 23, 1955

REFERENCES

1. Brun, Rinaldo J., Gallagher, Helen M., and Vogt, Dorothea E.: Impingement of Water Droplets on NACA 65A004 Airfoil and Effect of Change in Airfoil Thickness from 12 to 4 Percent at 4° Angle of Attack. NACA TN 3047, 1953.

2. Brun, Rinaldo J., Gallagher, Helen M., and Vogt, Dorothea E.: Impingement of Water Droplets on NACA 65A004 Airfoil at 8° Angle of Attack. NACA TN 3155, 1954.

3. Brun, Rinaldo J., Gallagher, Helen M., and Vogt, Dorothea E.: Impingement of Water Droplets on NACA 65_1-208 and 65_1-212 Airfoils at 4° Angle of Attack. NACA TN 2952, 1953.

4. Brun, Rinaldo J., and Mergler, Harry W.: Impingement of Water Droplets on a Cylinder in an Incompressible Flow Field and Evaluation of Rotating Multicylinder Method for Measurement of Droplet-Size Distribution, Volume-Median Droplet Size, and Liquid-Water Content in Clouds. NACA TN 2904, 1953.

5. Brun, Rinaldo J., Serafini, John S., and Gallagher, Helen M.: Impingement of Cloud Droplets on Aerodynamic Bodies as Affected by Compressibility of Air Flow Around the Body. NACA TN 2903, 1953.

6. Dorsch, Robert G., and Brun, Rinaldo J.: A Method for Determining Cloud-Droplet Impingement on Swept Wings. NACA TN 2931, 1953.

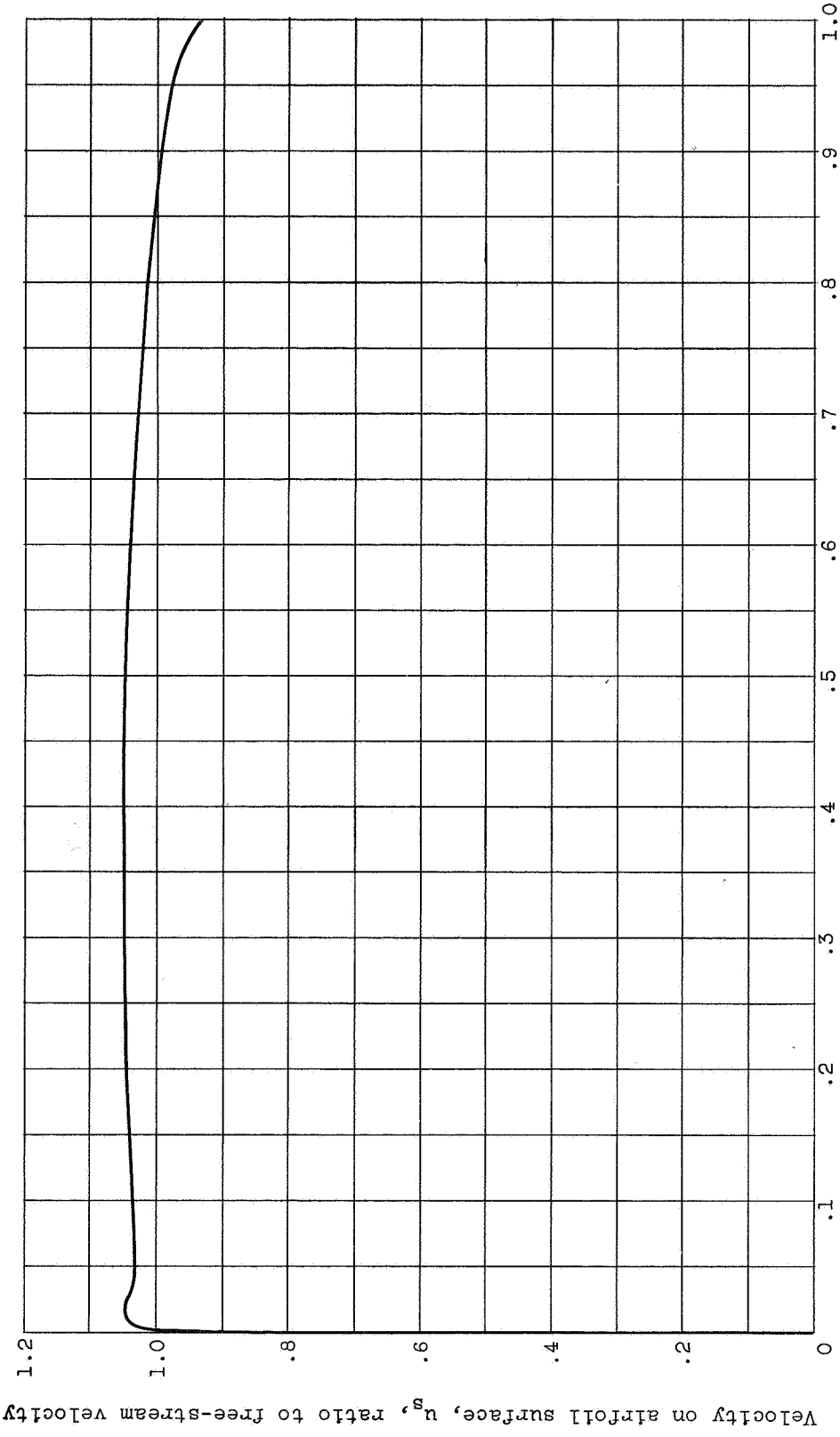

Figure 1. - Velocity distribution on surface of 65A004 symmetrical airfoil. Angle of attack, 0°; incompressible flow field.

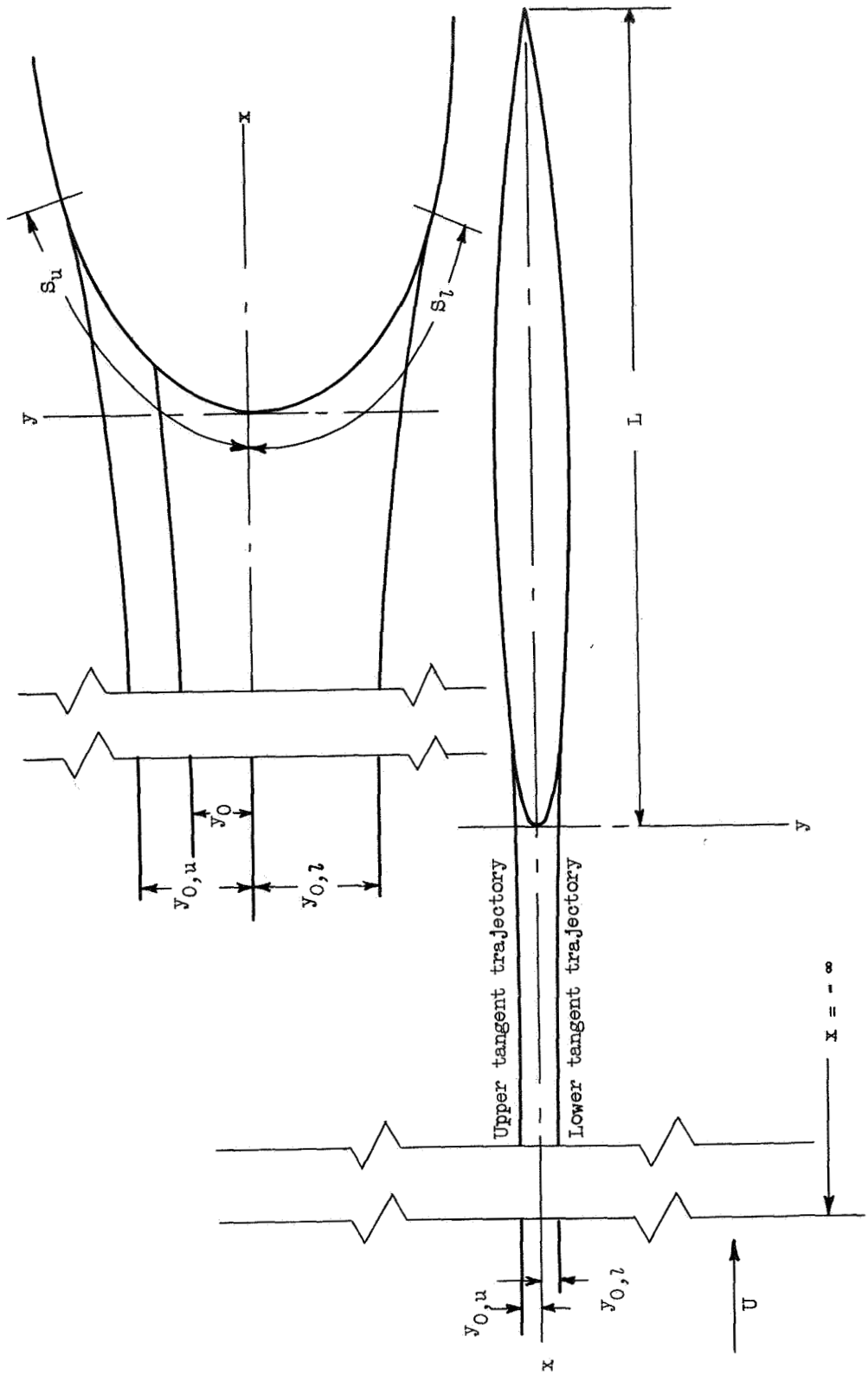

Figure 2. - Droplet trajectories with respect to airfoil.

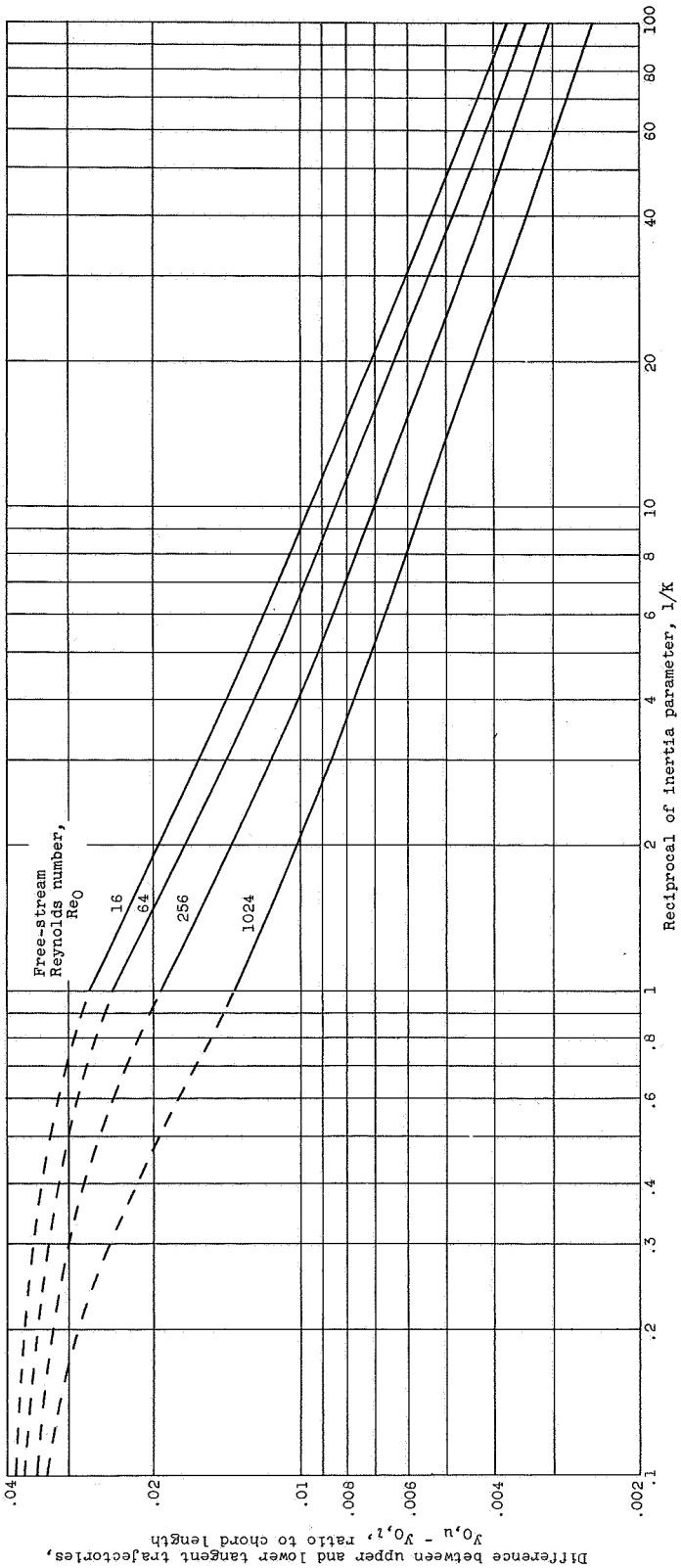

Figure 3. - Difference between starting ordinates of upper and lower tangent trajectories for 65A004 airfoil. Angle of attack; 0°.

(a) Droplet size, 15 microns. (b) Droplet size, 20 microns.

Figure 4. - Total rate of water impingement on 65A004 airfoil. Angle of attack, 0°; altitude, 20,000 feet; most probable icing temperature, -11° F.

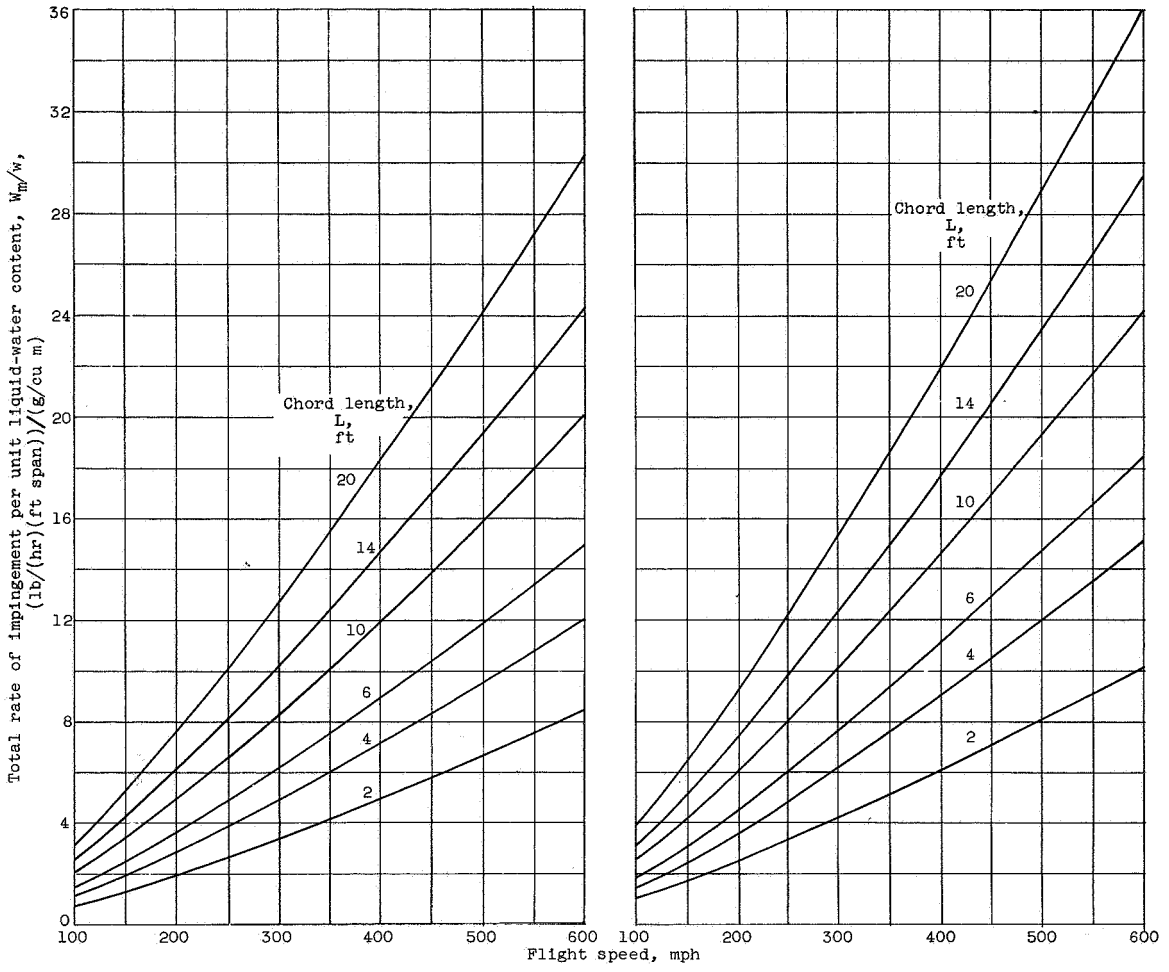

(c) Droplet size, 30 microns.

(d) Droplet size, 40 microns.

Figure 4. - Concluded. Total rate of water impingement on 65A004 airfoil. Angle of attack, 0°; altitude, 20,000 feet; most probable icing temperature, - 11° F.

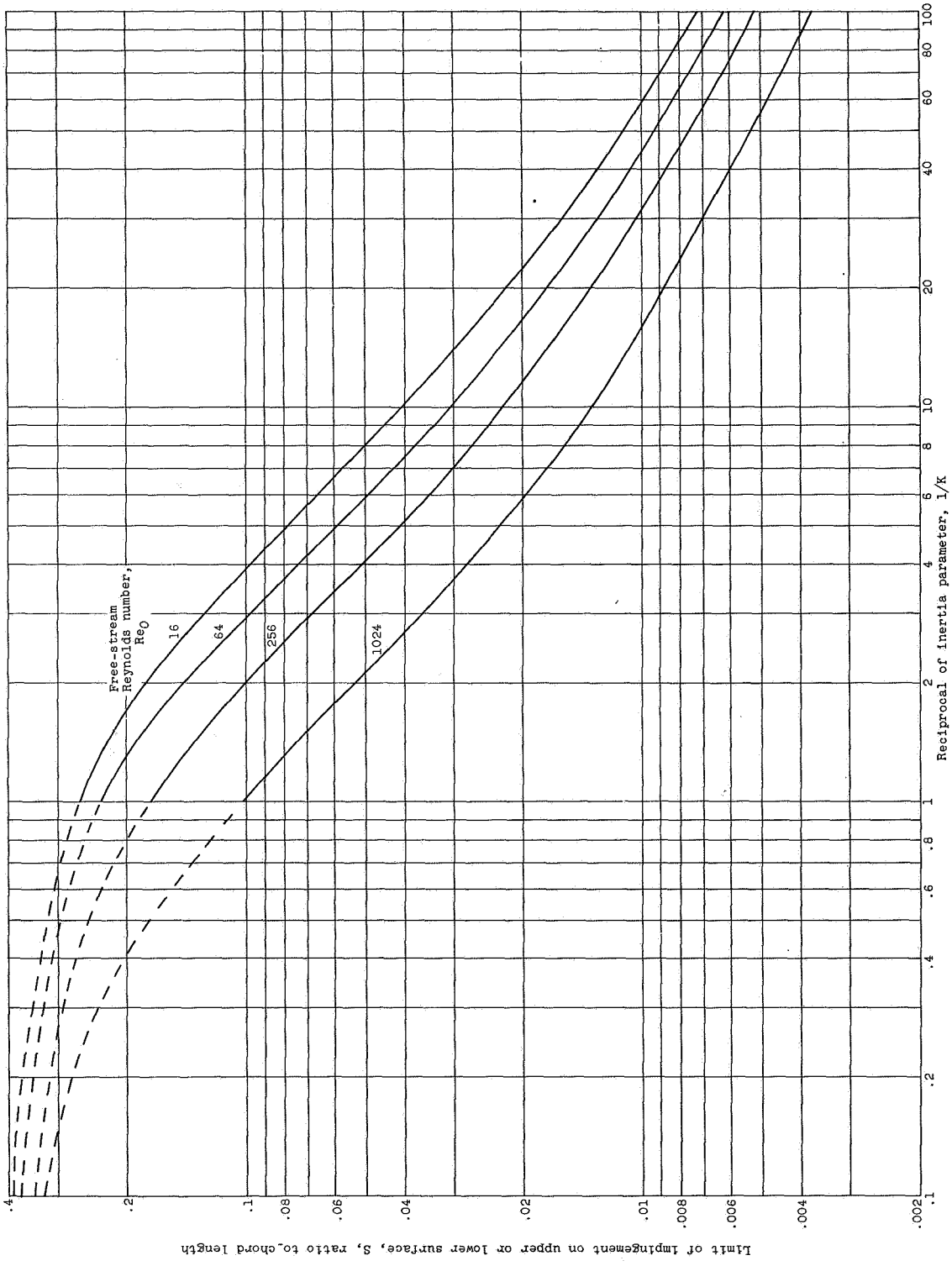

Figure 5. - Limit of impingement on upper or lower surface of 65A004 airfoil. Angle of attack, 0°.

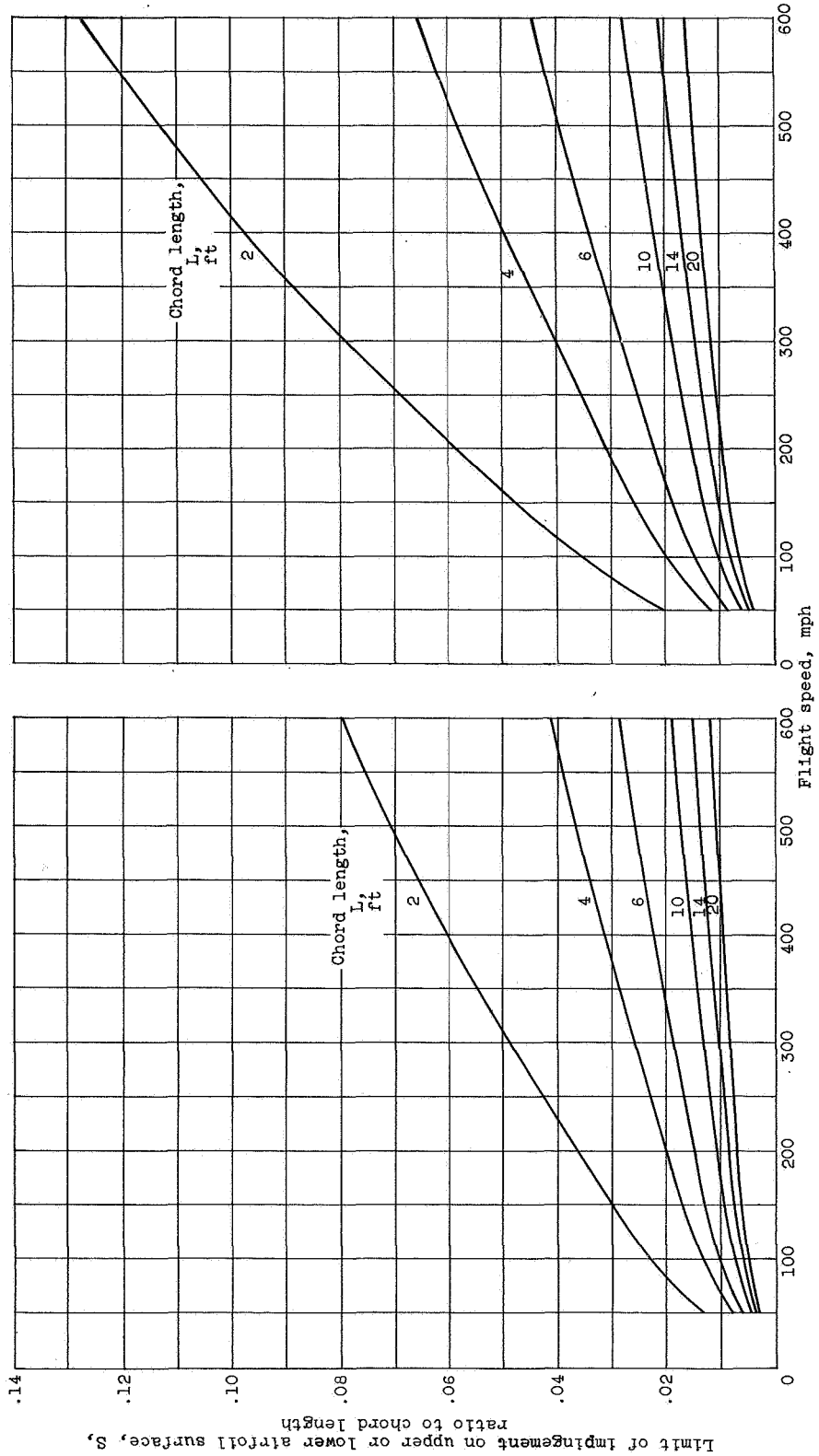

(a) Droplet size, 15 microns.

(b) Droplet size, 20 microns.

Figure 6. - Limit of impingement on upper or lower surface of 65A004 airfoil. Altitude, 20,000 feet; angle of attack, 0°; most probable icing temperature, -11° F.

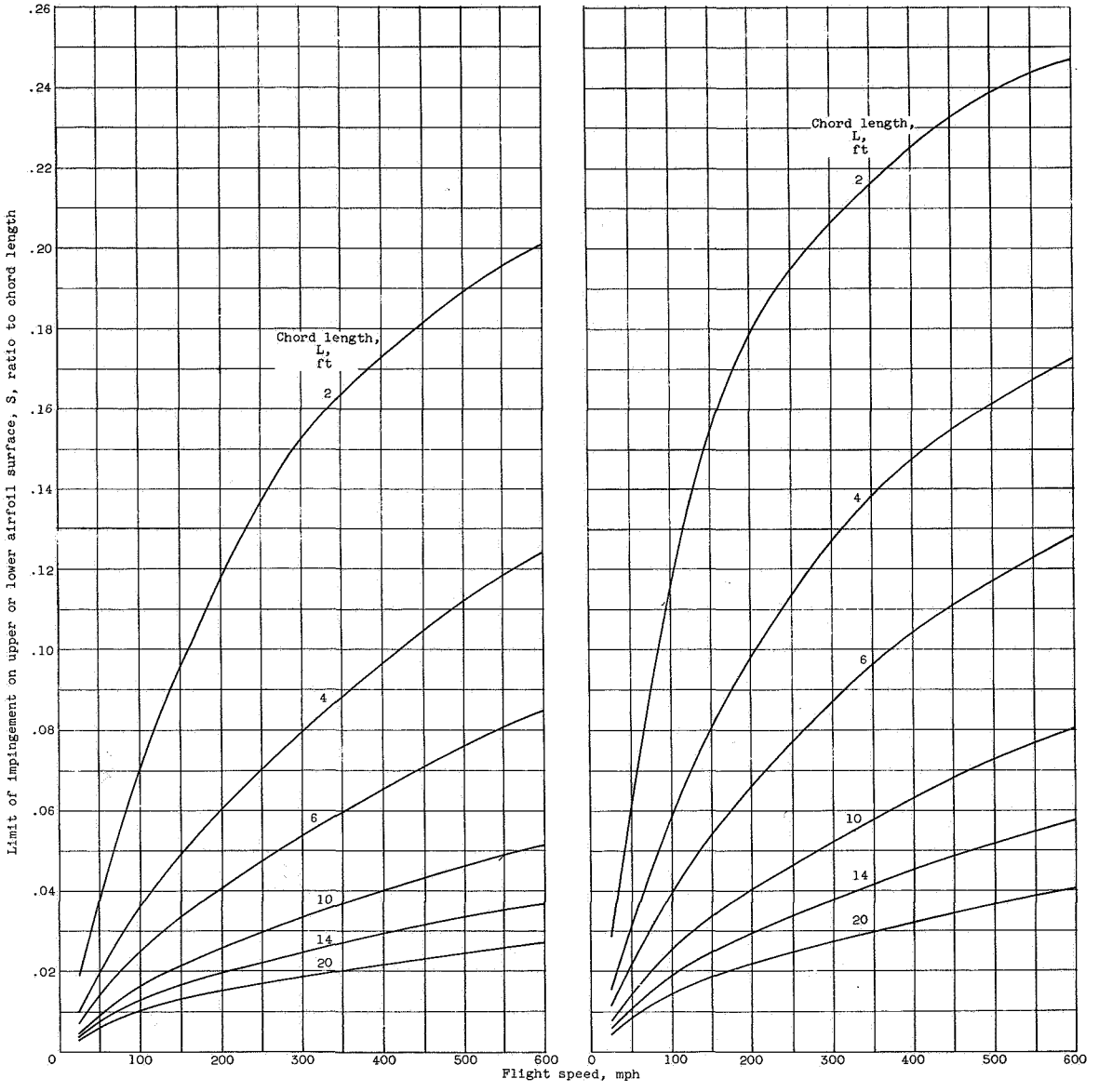

(c) Droplet size, 30 microns.

(d) Droplet size, 40 microns.

Figure 6. - Concluded. Limit of impingement on upper or lower surface of 65A004 airfoil. Altitude, 20,000 feet; angle of attack, 0°; most probable icing temperature, -11° F.

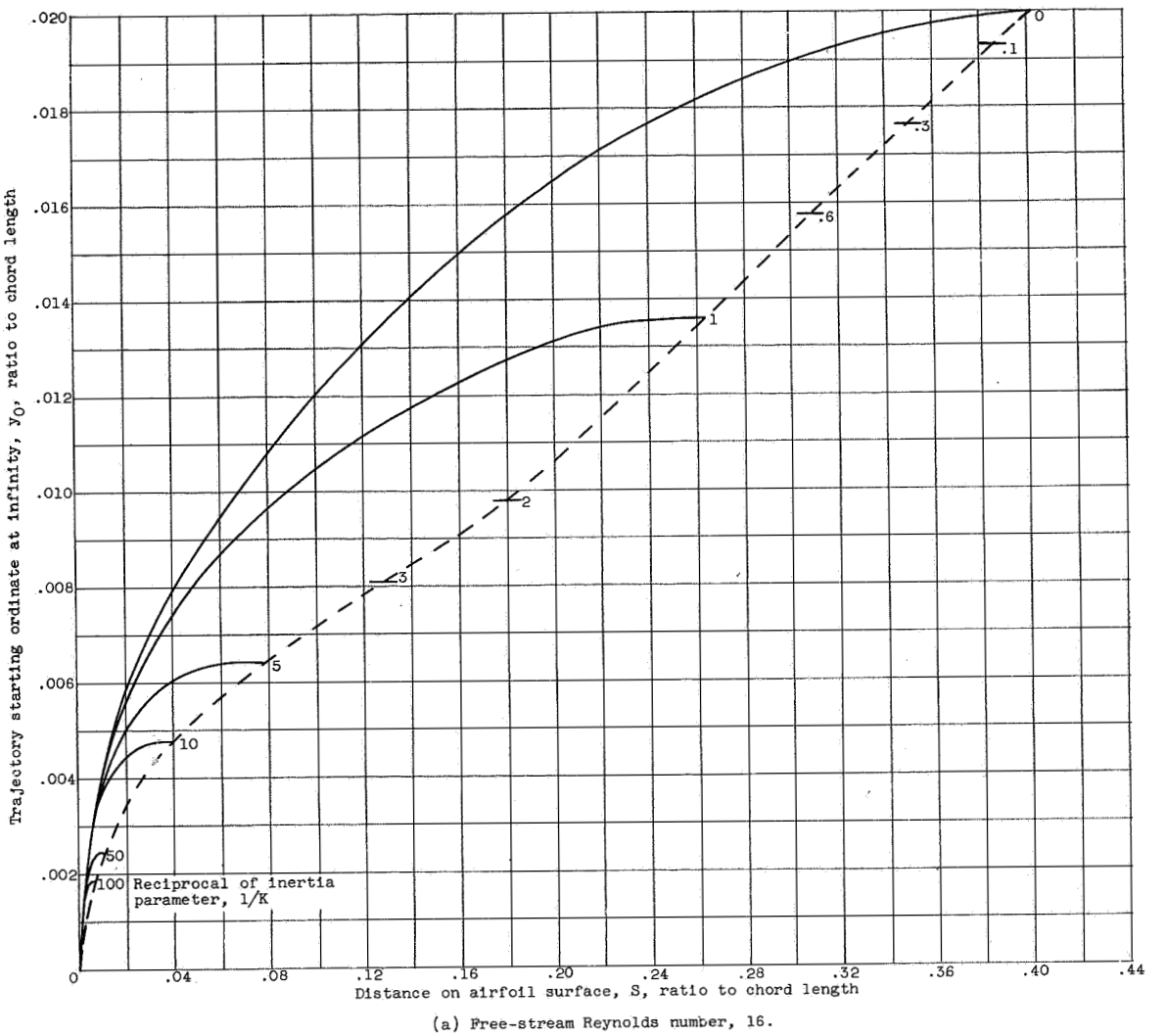

(a) Free-stream Reynolds number, 16.

Figure 7. - Trajectory starting ordinates as function of point of impingement on surface of 65A004 airfoil. Angle of attack, 0°.

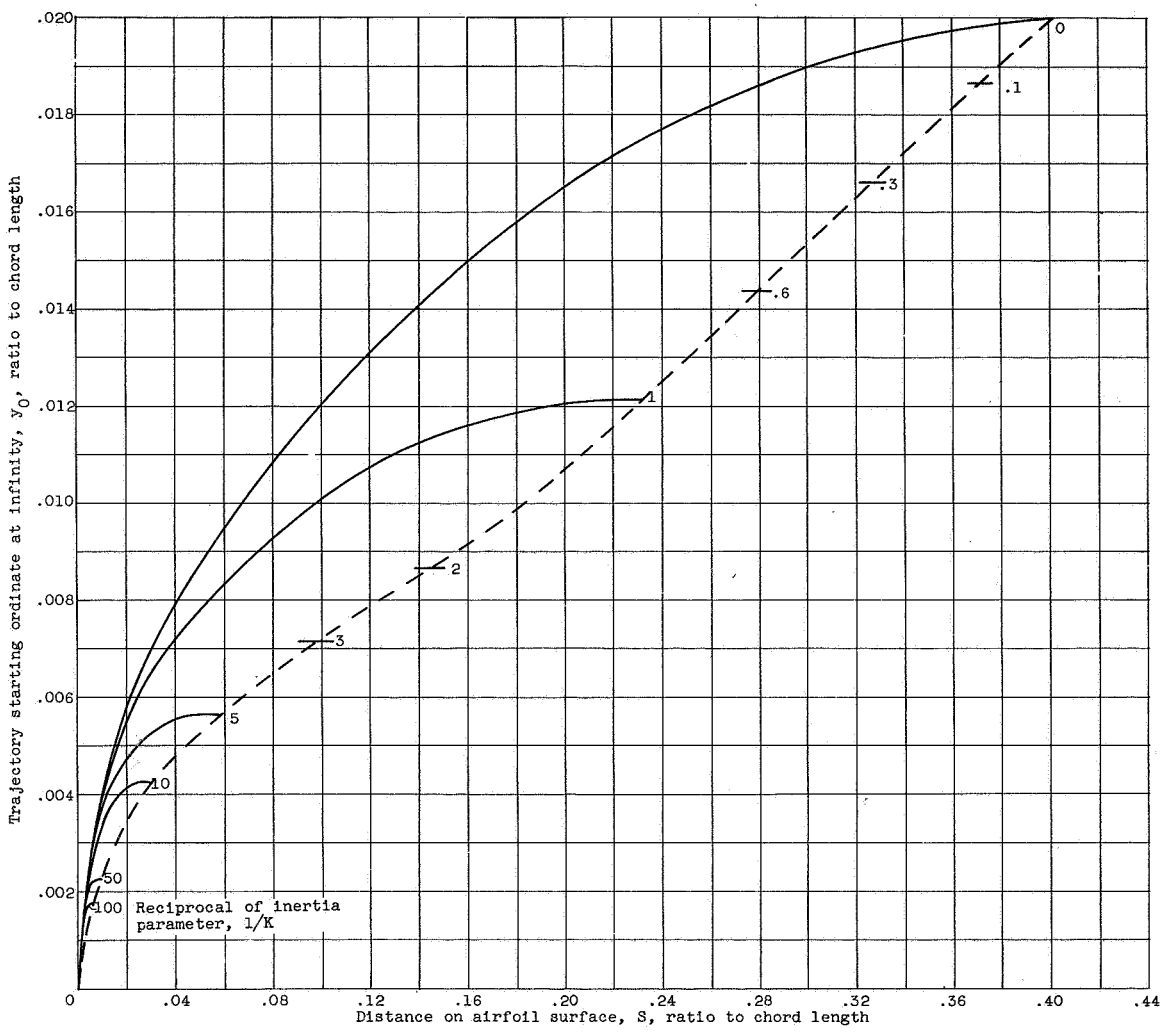

(b) Free-stream Reynolds number, 64.

Figure 7. - Continued. Trajectory starting ordinates as function of point of impingement on surface of 65A004 airfoil. Angle of attack, 0°.

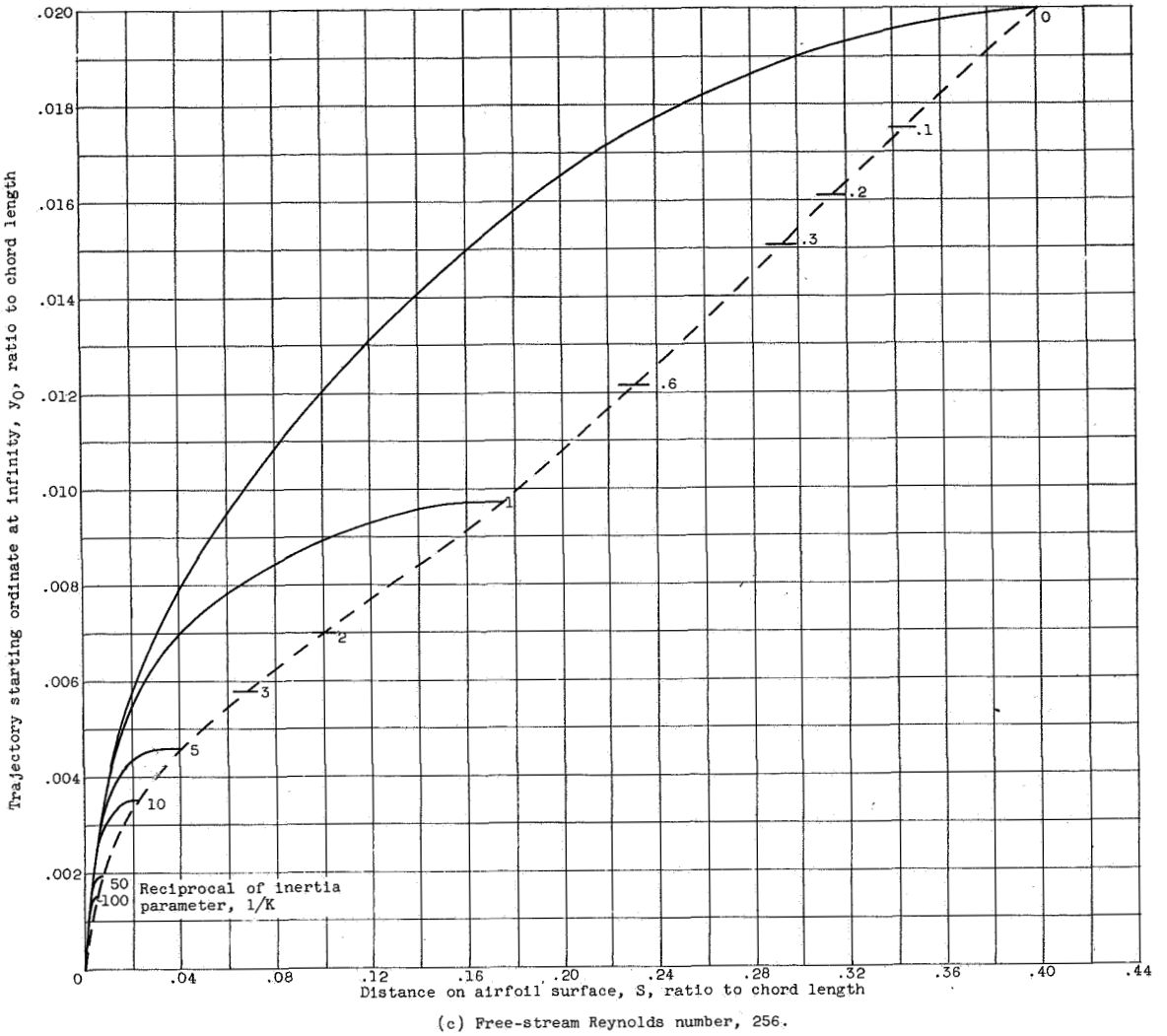

(c) Free-stream Reynolds number, 256.

Figure 7. - Continued. Trajectory starting ordinates as function of point of impingement on surface of 65A004 airfoil. Angle of attack, 0°.

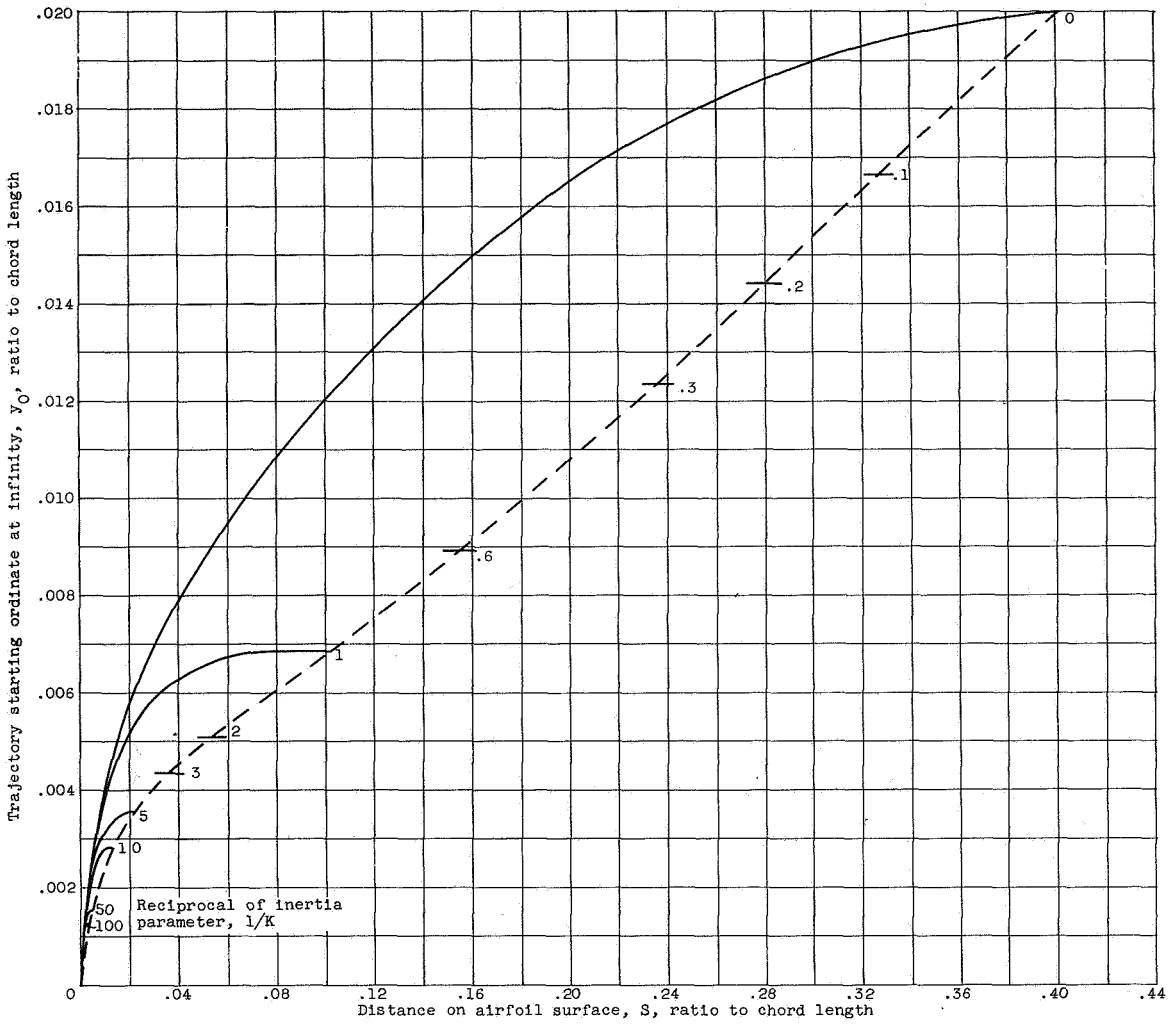

(d) Free-stream Reynolds number, 1024.

Figure 7. - Concluded. Trajectory starting ordinates as function of point of impingement on surface of 65A004 airfoil. Angle of attack, 0°.

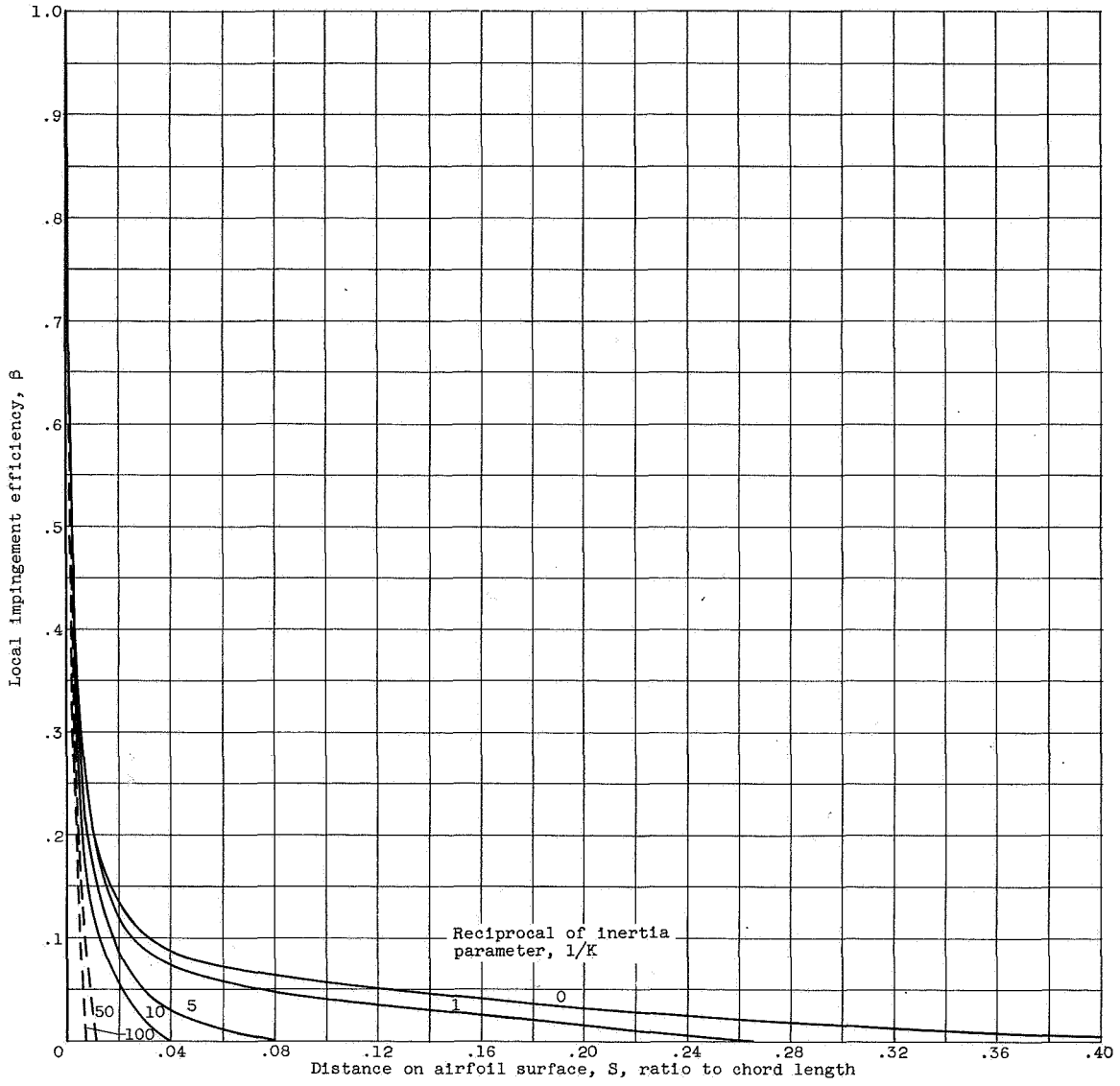

(a) Free-stream Reynolds number, 16.

Figure 8. - Local impingement efficiency of NACA 65A004 airfoil. Angle of attack, 0°.

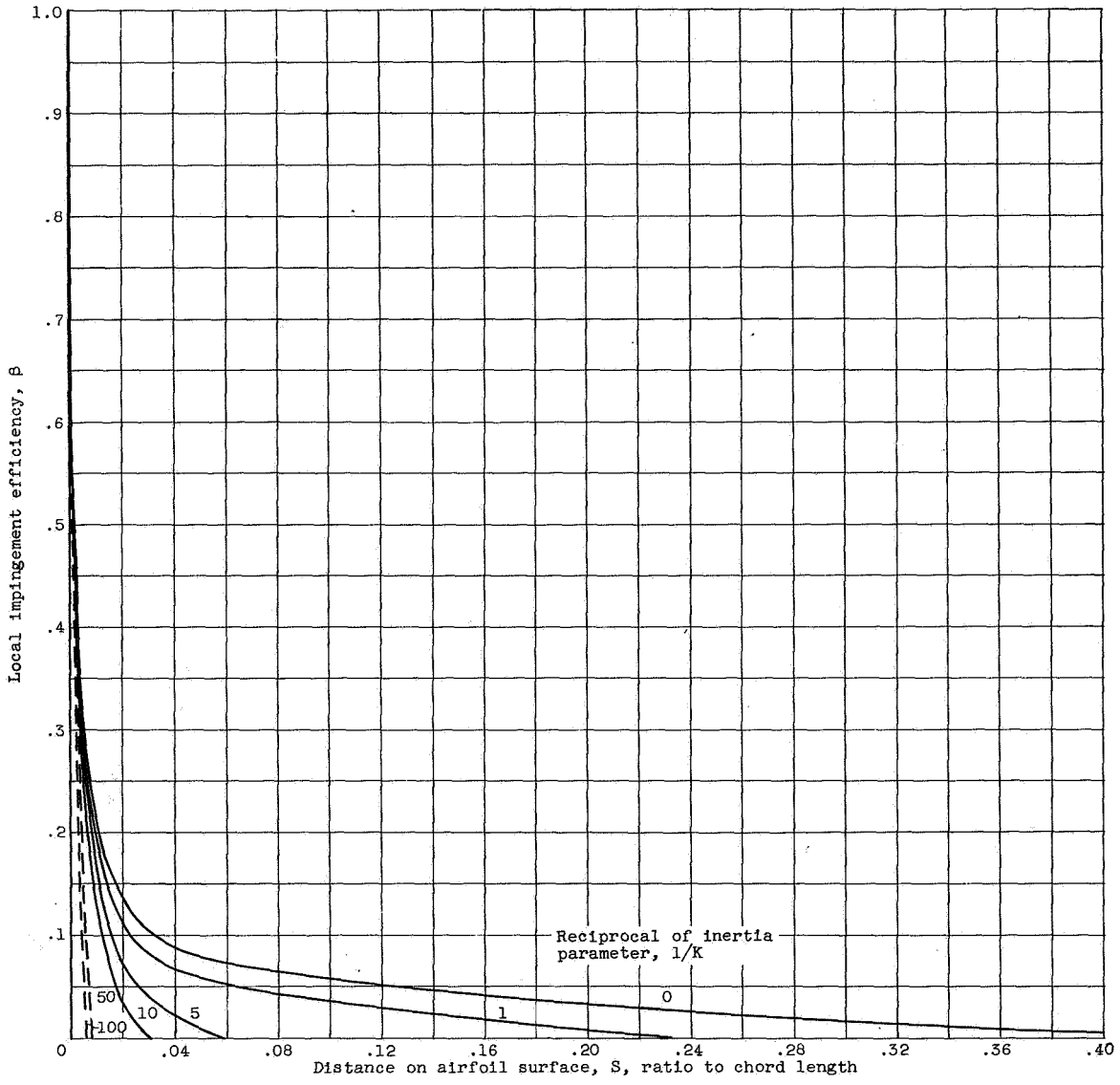

(b) Free-stream Reynolds number, 64.

Figure 8. - Continued. Local impingement efficiency of NACA 65A004 airfoil. Angle of attack, 0°.

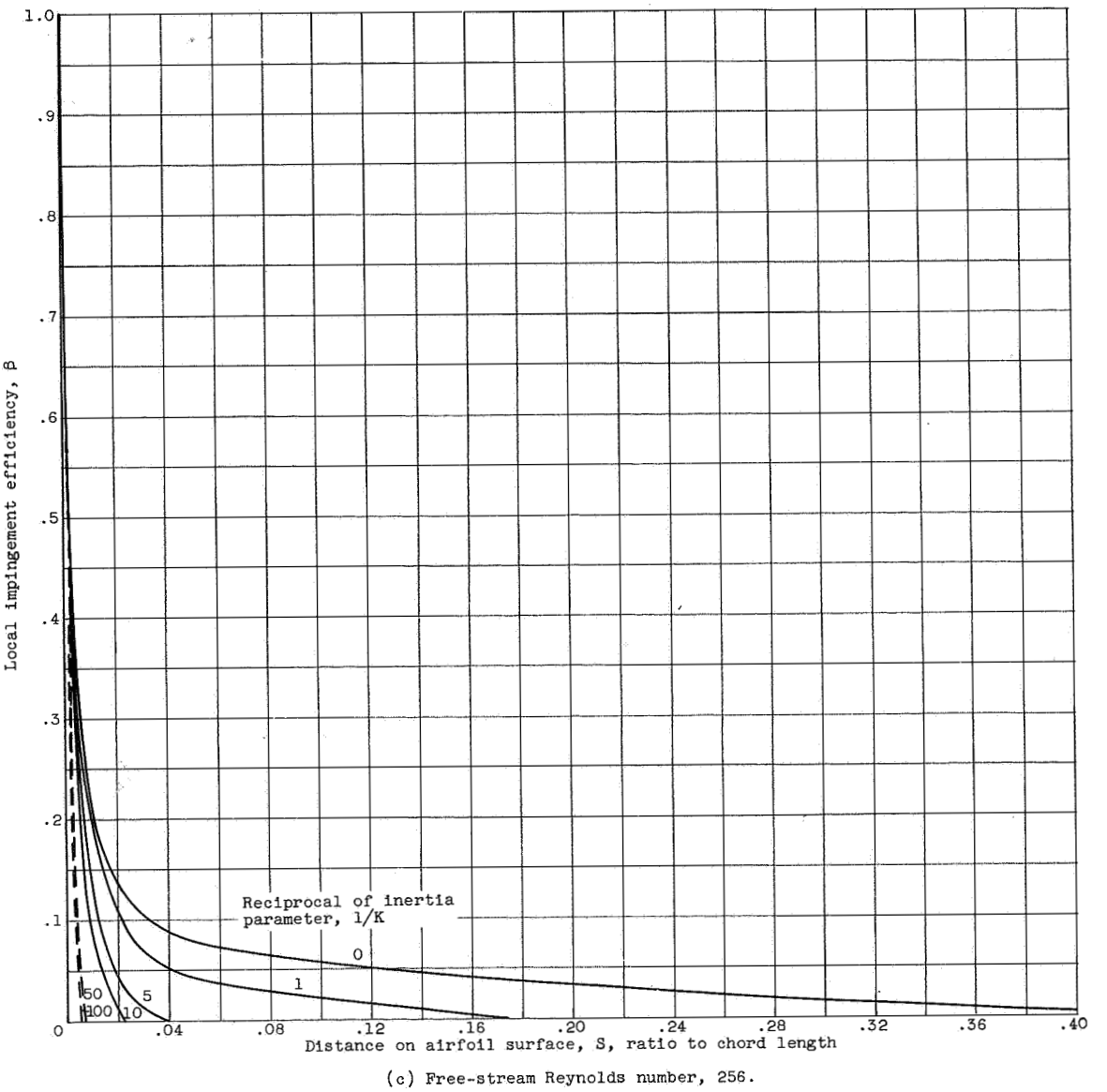

(c) Free-stream Reynolds number, 256.

Figure 8. - Continued. Local impingement efficiency of NACA 65A004 airfoil. Angle of attack, 0°.

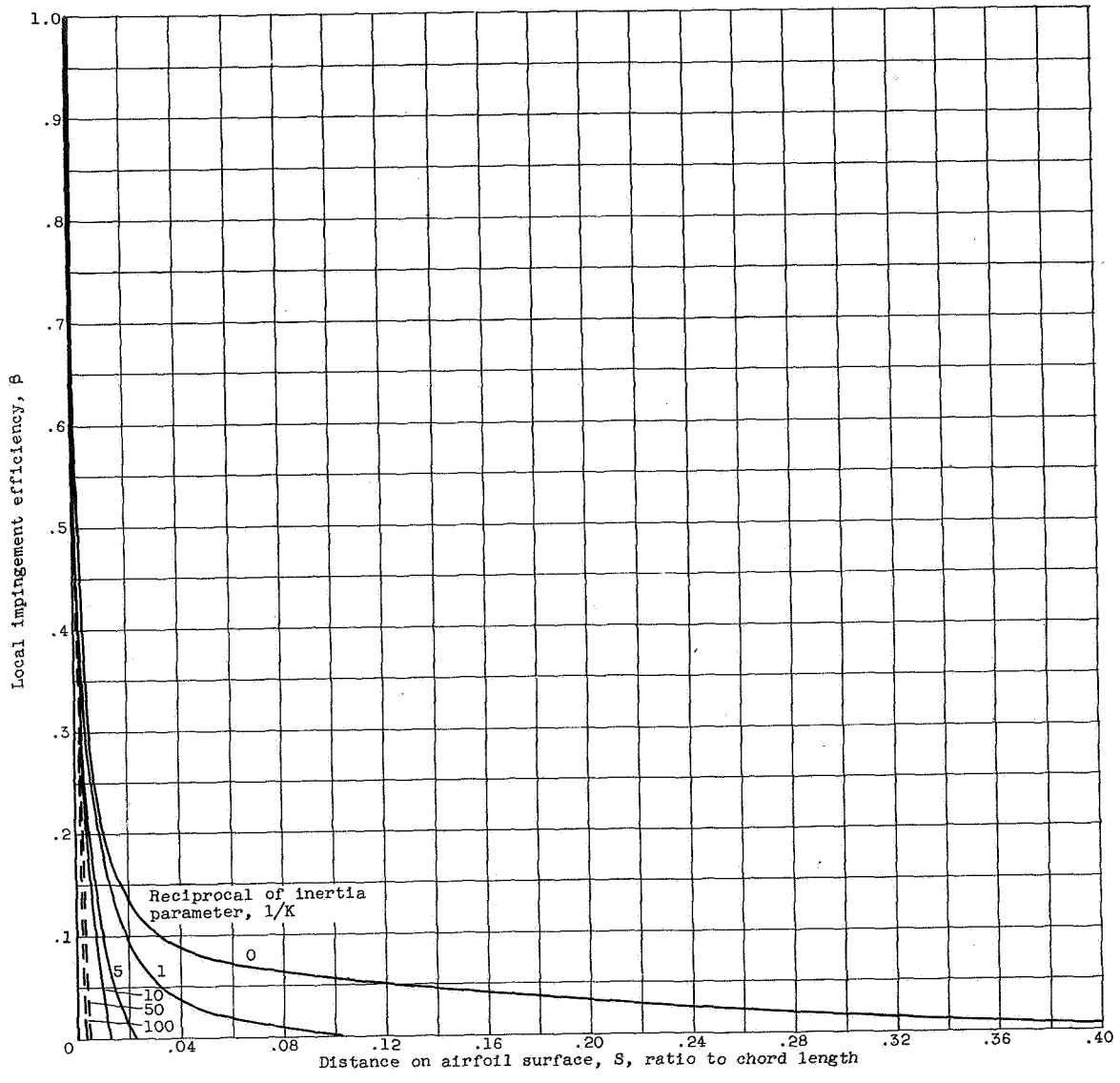

(d) Free-stream Reynolds number, 1024

Figure 8. - Concluded. Local impingement efficiency of NACA 65A004 airfoil. Angle of attack, 0°.

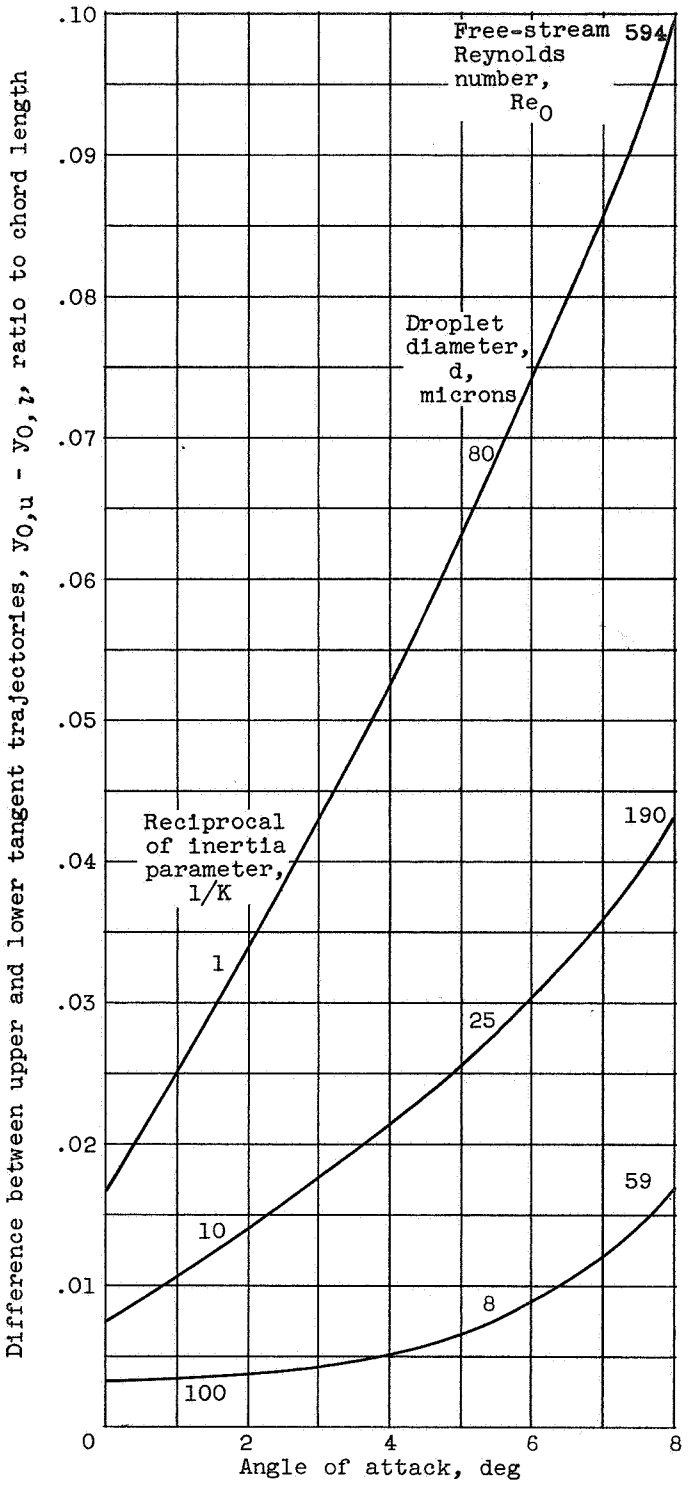

Figure 9. - Difference between tangent trajectories as function of angle of attack. Flight speed, 300 mph; chord length, 9.4 feet; altitude, 10,000 feet.

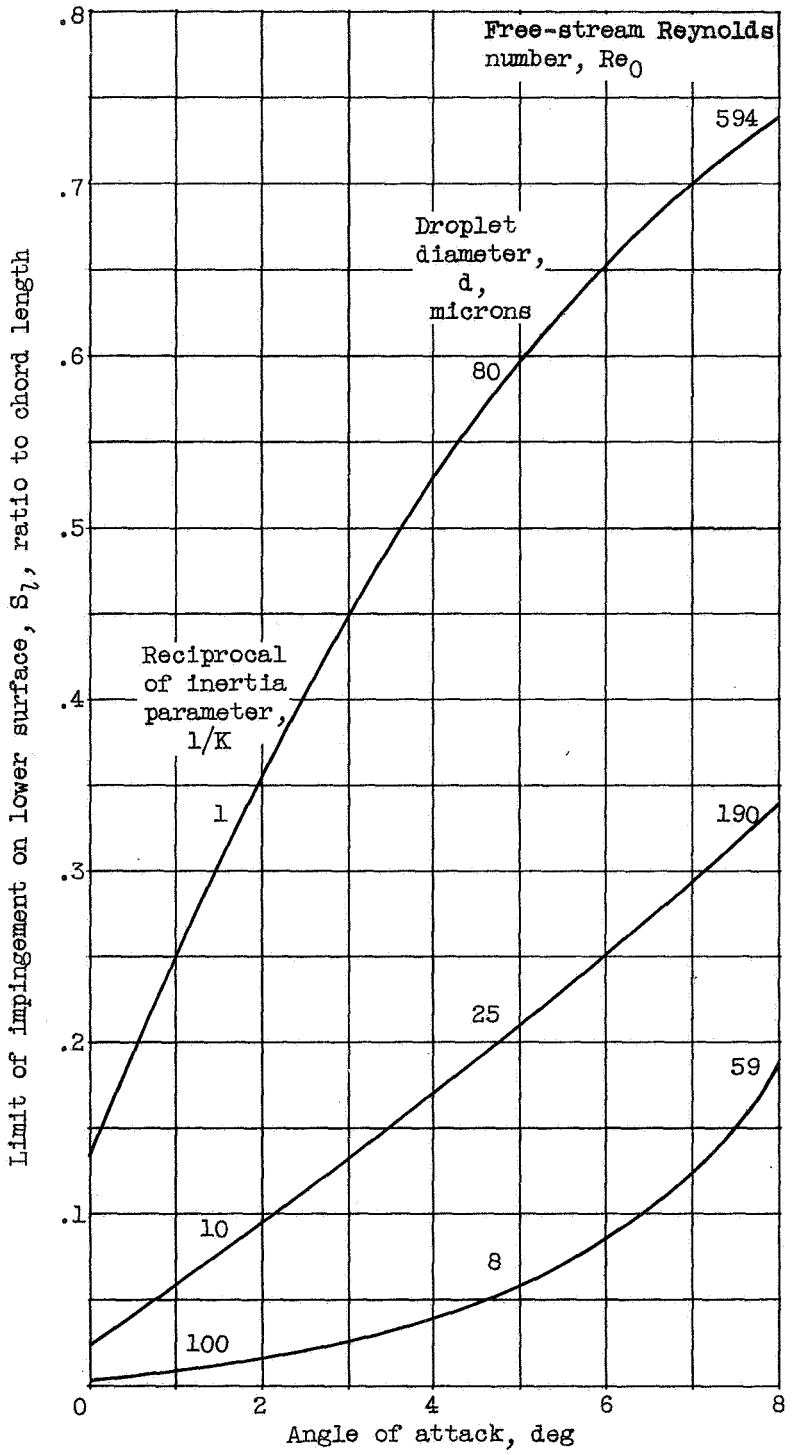

Figure 10. - Lower-surface impingement as function of angle of attack. Flight speed, 300 mph; chord length, 9.4 feet; altitude, 10,000 feet.